Collective beam-beam effects in hadron colliders

J. Shi and D. Yao
Department of Physics and Astronomy, The University of Kansas, Lawrence, Kansas 66045
(Received 27 December 1999)

Collective beam-beam effects in hadron colliders were studied with a strong-strong beam-beam simulation on the CERN Large Hadron Collider, including multipole field errors in the lattice and beam-beam interactions at two high-luminosity interaction points. It was found that the beam-beam interaction could result in two distinct dynamics for hadron beams: a slow beam-size growth and an unstable beam-centroid oscillation. The instability of the beam-centroid oscillation has typical characteristics of the chaotic transport, i.e., the amplitude increase of the oscillation consists of slow escape from the remnants of invariant manifolds and fast diffusion in fully developed chaotic regions. The simulation results indicate that there is a threshold of the beam-beam parameter below which no unstable beam-centroid motion was observed. The escape rate of the unstable beam-centroid motion, on the other hand, increases with the nonlinear field errors in the lattice. As the slow beam-size growth is strongly enhanced by the beam-centroid oscillation, an elimination of the centroid motion with feedback can effectively suppress the beam-size growth. No steady state of coherent beam-beam oscillation was observed.

PACS number(s): 29.27.−a, 29.20.−c, 41.85.−p

I. INTRODUCTION

In a colliding beam storage ring, the motion of particles in one beam is perturbed at the collision points by the electromagnetic field exerted by the counter-rotating beam. This beam-beam interaction is one of the sources of the growth of the transverse beam size, and limits the luminosity of storage rings. Since the evaluation of the beam-beam interaction requires a knowledge of beam-particle distributions that, in turn, evolve under the perturbation of the beam-beam interaction, a complete understanding of beam-beam effects requires a solution of the nonlinear Vlasov equation. As an exact formalism for a direct calculation of this time-dependent nonlinear collective effect is not available, the study of the beam-beam effects has mostly relied on particle tracking. Due to the difficulty of computing the particle distribution during the tracking, the beam-beam effects are conventionally studied with the strong-weak approximation, in which a few testing particles are tracked with a time-independent beam-beam force, usually with the assumption of a Gaussian distribution for the beam-beam force. Although such a single-particle description has provided some useful insight into the nature of nonlinear resonances of the beam-beam effects, and has been a conventional method for a routine check of the dynamic aperture of a colliding beam storage ring, the validity of this strong-weak approximation has not been well understood for two colliding beams of similar emittance. Moreover, the strong-weak simulations cannot provide an insight into the collective nature of the beam-beam effects that could be important to the limitation of the luminosity of a colliding beam storage ring [1].

The collective (or coherent) beam-beam effects are characterized by coherent oscillations of the particle distributions of two colliding beams, and have been observed in electron storage ring colliders [1,2]. One such example is the flip-flop instability in which beams that start out with equal transverse beam sizes end up in a steady state with very unequal beam size. Because of the reduction of the overlap between the beams, the luminosity is reduced by this coherent beam-beam effect. Two different types of theoretical models have been proposed for understanding the coherent beam-beam instabilities in electron storage ring colliders [3–5]. In the first type of model nonlinear maps for the moments of beams are obtained by a truncation of a moment expansion for the distribution functions, while in the second the type of model instabilities of an equilibrium distribution of beams are analyzed with the linearized Vlasov equation. In both models, steady states of the coherent oscillations were obtained. For a high-energy electron beam, because of the radiation effect, the time required for a beam to reach equilibrium distribution is much less than the storage time. Consequently, the study of beam dynamics can be focused on the behavior of the distribution near its steady states. Moreover, a fast damping of high-order fluctuations permits a truncation of the moment expansion at fairly low orders. On the other hand, self-consistent computer simulations of the beam-beam interaction (strong-strong beam-beam simulation) have also been conducted for electron beams in a linear ring by using the particle-in-cell method [6–9]. Coherent beam-beam instabilities were observed in the simulations, and the results agreed qualitatively with the theoretical models.

Contrary to electron storage ring colliders, much less progress has been made toward an understanding of the collective beam-beam effects in hadron colliders. This is mainly due to the different behavior of the particle distributions in electron and hadron storage rings. For a high-energy hadron beam, the damping time is usually larger than the storage time, so that the motion of beam particles is determined by Hamiltonian dynamics. In the presence of nonlinear perturbations due to either beam-beam interactions or nonlinear field errors in the lattice, the particle distribution may not reach any steady state within a fraction of the storage time. Consequently, approximations of the truncation of high-order moments for the moment map or the linear stability analysis of equilibrium distributions of the Vlasov equation are no longer valid. Experimentally, since the time scale for the relaxation is much longer than the time scale of the observation, it may not be possible to observe a stationary co-

herent oscillation of beam-beam effects in hadron colliders. On the other hand, the lack of damping makes the slow beam-size growth important in hadron colliders. Observations have shown that the growth of tails of the particle distribution is a serious problem, as it enhances the background level in detectors. The methods of perturbation expansion for the distribution function, using the techniques of multiple scales or projection operators, were found to be effective for studying the evolution of the particle distribution in hadron storage rings when weak nonlinear field errors were considered [10,11]. For beam-beam interactions, it is possible to obtain numerically a self-consistent perturbation expansion of the distribution function. The expansion procedure, however, becomes too complicated to be practical, especially with a strong nonlinear perturbation. Considering the case of weak beam-beam perturbation, Alexahin [12] and Kokoya *et al.* [13] studied coherent oscillation with the linearized Vlasov equation, with the assumption that the equilibrium distribution is a Gaussian in action variables. These studies provided many insights into the characteristics of the beam filamentation when a weak (nearly integrable) beam-beam perturbation is considered. Many questions on the beam-beam instability that usually occurs in a highly nonintegrable regime remain open. In order to have a better understanding of the collective beam-beam effects and the slow beam-size growth of hadron beams, a strong-strong beam-beam simulation needs to be conducted for hadron colliders. Since for large hadron colliders the magnetic-field error in the lattice is the major nonlinearity besides the beam-beam interaction, and it plays an important role in beam-size growth, the simulation of the beam-beam effects should also include nonlinear fields in the lattice.

In a strong-strong beam-beam simulation, the beam-beam force exerted on each beam needs to be calculated self-consistently during the tracking. One way to evaluate this self-consistent beam-beam force is the particle-in-cell method, that has been widely used for simulations with particles in computational plasma physics and computational cosmology [14,15], and has also been used for strong-strong beam-beam simulation in electron storage ring colliders [6–9]. In the tracking of particles with the particle-in-cell method, a number of macroparticles is distributed in the phase space initially for each beam according to the initial distribution of beams. When the beams cross an interaction point during the tracking, the beam-beam force for each beam is calculated on a mesh in a configuration space based on the density of macroparticles of the counter-rotating beam. In order to produce a reliable tracking result, a sufficiently large number of macroparticles has to be used. Our study showed that the number of macroparticles needed for the study of the slow beam-size growth in hadron colliders is much larger than that for the strong-strong beam-beam simulation in electron storage ring colliders.

In this paper we study the strong-strong beam-beam effects of proton beams in the CERN LHC (large hadron collider), including magnetic field errors in the lattice and beam-beam interactions at two high-luminosity interaction points, by using the particle-in-cell method. It was found that beam-beam interactions can result in a slow beam-size growth and an unstable oscillation with chaotic transport of beam centroids. As the beam-size growth is enhanced by a chaotic oscillation of the beam centroids, the elimination of the centroid motion with feedback can effectively suppress the beam-size growth. This paper is organized as follows. In Sec. II, the test lattice for the LHC during collisions is presented and the particle-in-cell method for the strong-strong beam-beam simulation is discussed. The results of strong-strong beam-beam simulation of proton beams in the LHC are presented in Sec. III. Section IV contains a summary.

II. SIMULATION MODEL

A. Test lattice

The test lattice used in this study is the LHC version 5.0 [16]. The LHC has four interaction regions (IR's): IR1 and IR5 are high-luminosity interaction points ($\beta^* = 0.5$ m), and IR2 and IR8 are low-luminosity points. Each inner triplet of IR's comprises four superconducting high gradient quadrupoles: $Q1$, $Q2A$, $Q2B$, and $Q3$. Due to the beam separation and the large β functions, the dominant nonlinearities in the ring at collision energy are the field errors of the high gradient quadrupoles in IR's. Since β_{max} ($\sim$4700 m) in the triplets of IR1 and IR5 is more than ten times larger that of IR2 and IR8, the field quality in the triplets of IR1 and IR5 is far more important than that of IR2 and IR8. In this study we therefore consider only those field errors of the quadrupoles in IR1 and IR5. Both KEK and Fermilab will build 16 of these 32 IR quadrupoles. Reference harmonics of version 2.0 for Fermilab quadrupoles and of version 3.0 for KEK quadrupoles are used in this study [17,18]. All multipoles up to ninth order in the field errors are included. The uncertainty of a systematic error in the error tables is simply added to the systematic error in such a way that it maximizes the systematic error. The random multipole components of the field errors are chosen with Gaussian distributions centered at zero, and truncated at $\pm 3\sigma_{b_{n+1}}$ or $\pm 3\sigma_{a_{n+1}}$, where $\sigma_{b_{n+1}}$ and $\sigma_{a_{n+1}}$ are the rms values of the nth-order normal and skew multipole coefficient (in the European convention), respectively. Due to the consideration of a larger systematic b_{10} in KEK quadrupoles, the mixed configuration is adapted, i.e., the Fermilab quadrupoles are installed at $Q2A$ and $Q2B$ and the KEK quadrupoles at $Q1$ and $Q3$ [18]. To compensate for the field errors in the IR's, correctors in each IR are proposed for eliminating the multipole field errors up to b_6 and a_6 [18]. In this study, the crossing angle of two counter-rotating beams is taken to be 300 μrad, which is the current nominal LHC value. The lattice is linearly decoupled globally and locally at the high-luminosity interaction points (IP1 and IP5). The fractional parts of horizontal and vertical tunes of the LHC are $\nu_x = 0.31$ and $\nu_y = 0.32$, respectively. Tracking of particle motion has been done without synchrotron oscillations and momentum deviations.

Without beam-beam interactions, the dynamic aperture of the LHC collision lattice is calculated with 10^5-turn tracking on 100 different samples of random field errors generated with different seed numbers in a random number generator routine. Without any IR corrector, the worst case of these 100 samples has a dynamic aperture of 6σ, where σ is the transverse beam size. At IP1 and IP5, $\sigma = 15.9$ μm. With local IR correctors of b_n and a_n for $n = 3$, 4, 5, and 6 in each triplet, the dynamic aperture of this case becomes 11σ. In the

following, we use this sample for the strong-strong beam-beam simulation. Since head-on beam-beam interactions are the dominant beam-beam perturbations at beam cores, they are more important than the long-range beam-beam interactions for the collective beam-beam effects. In this study, only head-on beam-beam interactions at IP1 and IP5 are included in the strong-strong beam-beam simulation.

B. Formulas for beam-beam interactions

Consider a head-on collision of two ultrarelativistic proton beams. Let $\rho(\vec{r})$ denote the particle density of one beam in normalized transverse configuration space, where $\vec{r}=(x,y)$ and the dimension of $\vec{r}$ is $m^{1/2}$. The beam-beam kick force in transverse phase space on a test particle in the counter-rotating beam is

$$\vec{K}(\vec{r})=\int d\vec{r'}\rho(\vec{r'})\vec{G}(\vec{r}-\vec{r'}), \tag{1}$$

where

$$\vec{G}(\vec{r}-\vec{r'})=G_0\frac{(\vec{r}-\vec{r'})}{(x-x')^2+(y-y')^2} \tag{2}$$

is the Green's function for the beam-beam kick and $G_0=2Nr_p/\gamma$. N is the number of protons per bunch, r_p the classical proton radius, and γ the relativistic factor. Equation (1) can be directly used for the field calculation in the strong-strong beam-beam simulation. For the case of a round beam that is Gaussian in both transverse coordinates with standard deviations $\sigma_x=\sigma_y=\sigma_0$, the kick force becomes

$$\vec{K}(\vec{r})=\frac{G_0\vec{r}}{r^2}\left[1-\exp\left(-\frac{r^2}{2\sigma_0^2}\right)\right]. \tag{3}$$

Note that the dimension of σ_0 is $m^{1/2}$. The beam-beam kick in Eq. (3) is usually employed in the strong-weak beam-beam simulation for round beams. The strength of the beam-beam interaction can be conveniently parametrized by the beam-beam tune shift (beam-beam parameter) that is defined by $\xi=Nr_p/4\pi\epsilon_n$ where ϵ_n is the normalized transverse emittance. The kick strength G_0 is related to ξ by $G_0=8\pi\sigma_0^2\xi$.

C. Particle-in-cell method

In the strong-strong beam-beam simulation, each beam is represented by a large number of macroparticles distributed in transverse phase space and tracked for a large number of turns, with each turn consisting of transport between the interaction points and beam-beam collisions. In this study, the initial phase-space distributions of two counter-rotating beams are chosen to be identical round Gaussian beams in the normalized transverse phase space with standard deviation σ_0, and truncated at $\pm 4\sigma_0$, where $\sigma_0=\sigma/\sqrt{\beta^*}$. σ and β^* are the LHC nominal transverse beam size and the value of the β function at the interaction point, respectively.

The self-consistent beam-beam interactions at the collision points are calculated by using the particle-in-cell method, in which the electromagnetic fields are calculated on a rectangular mesh in transverse configuration space for each beam. This task consists of three major steps: (a) The charge distributions on the meshes are first obtained by assigning the macroparticles to the grid points using a four-point cloud-in-cell technique [14]. (b) The fields are calculated at the grid points by using Eq. (1), with precalculated Green's functions of Eq. (2). (c) The fields are then interpolated to the position of every macroparticle. In order to preserve the conservation of momentum, the same cloud-in-cell technique is employed for the interpolation of the fields and the assignment of the charge distributions. If the number of macroparticles is N_m and the number of the grid points N_g, the number of computer operations needed for each beam-beam crossing is proportional to $N_mN_g^2$. It should be noted that the field calculation in step (b) can also be done by solving the Poisson equation for the electric potential with a partial-differential-equation solver [15]. For larger values of N_g, this method has an advantage in computational speed as the number of calculations goes as $N_mN_g\ln_2 N_g$ for each beam-beam crossing [15]. On the other hand, since there is no boundary condition involved in the beam-beam interactions, the fields can be directly calculated from Eq. (1) with better accuracy. In order to keep N_g not too large, however, the mesh has to be terminated at a certain point in the configuration space. For the beam-beam simulation, the mesh should be large enough to cover the beam core. As a matter of fact, the particles in the beam tails have very little effect, and only respond to the beam-beam force. In particular, they have very little forces on the collective beam-beam effects. For the particles in the tails that are not covered by the meshes, a strong-weak calculation of the beam-beam force is therefore used.

In the numerical implementation, the size of the mesh and the grid constant (the length between nearest neighboring grid points) have to be carefully tested. To choose the size of the mesh, we monitor the number of macroparticles that escape to the outside of the mesh, and require this number to be small (negligible) compared to the total number of macroparticles. The grid constant, on the other hand, should be much smaller than σ_0. However, it cannot be too small for a given number of macroparticles, otherwise one may have a very non-smooth charge distribution function because the number of particles falling in a cell becomes small, which will result in significant fluctuations from cell to cell. The criterion here is that the initial field calculated by using the particle-in-cell method deviates as little as possible from the exact initial field. To obtain a reliable result, these simulation parameters were also tested, such that the tracking results are robust when the parameters vary around the chosen values. In this study, we found that a uniform mesh extending to $6\sigma_0$ in all directions of the normalized configuration space is good enough. The grid constant was chosen to be $0.2\sigma_0$.

For a given mesh, there is a minimum number of macroparticles above which the tracking results tend to be independent of the number of particles. Figure 1 plots the percentage increase of horizontal rms emittance of one beam calculated with $N_m=10^4$, 10^5, 5×10^5, and 10^6. The horizontal rms emittance is defined as $\epsilon_x=\langle x^2+p_x^2\rangle/2$, where x and p_x are the normalized horizontal coordinate and the momentum, respectively, and $\langle\cdots\rangle$ denotes the average over all the particles in each bunch. The vertical rms emittance is defined in a similar way. ϵ_0 is the initial emittance that can be evaluated

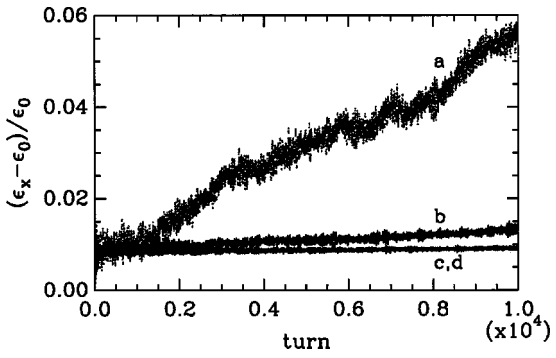

FIG. 1. Evolution of the horizontal rms emittance in LHC calculated by a particle-in-cell simulation with (a) 10^4, (b) 10^5, (c) 5×10^5, and (d) 10^6 macroparticles. Note that curves for (c) and (d) overlap. The initial emittance is $\epsilon_0=\sigma^2/(2\beta^*)$. Magnetic field errors in the triplets and beam-beam interactions at IP1 and IP5 are included in the simulation. $\xi=0.0136$.

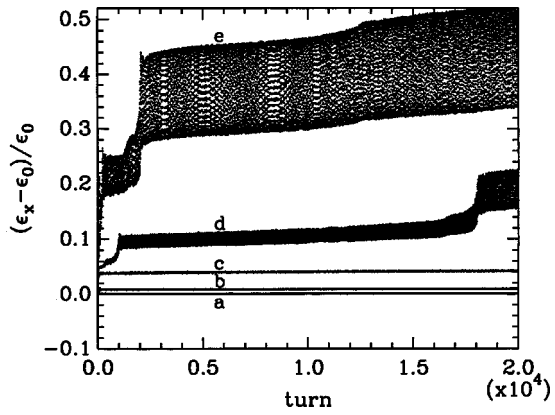

FIG. 2. Emittance growth when (a) $\xi=0.0034$, (b) $\xi=0.0136$, (c) $\xi=0.03$, (d) $\xi=0.034$, and (e) $\xi=0.04$. Magnetic field errors in the triplets and beam-beam interactions at IP1 and IP5 are included in the simulation.

by $\epsilon_0=\sigma^2/\beta^*$. Figure 1 clearly shows that the character of the emittance growth becomes independent of N_m only when $N_m\geqslant5\times10^5$ for a grid constant of 0.2σ. A plot of the vertical emittance or of the emittance of the counter-rotating beam shows a similar behavior. In order to have a reliable beam-beam simulation for proton beams, the number of macroparticles therefore has to be large enough. For high-energy electron beams, on the other hand, it has been reported that a much smaller number of macroparticles ($\sim10^4$) is possible for the strong-strong beam-beam simulation. The different requirement here could stem from the different behavior of the particle distribution in electron and hadron colliders. Since the dissipation of electron beams suppresses high-order fluctuations, the particle distribution tends to be smoother, and can be simulated with fewer particles. On the other hand, the lack of dissipation for hadron beams makes the fine structures of Hamiltonian dynamics important. Consequently, a larger number of particles is needed in order to obtain enough detailed information about the phase-space structures for the time scale of interest. In this study, the number of macro-particles was chosen to be 5×10^5.

III. SIMULATION RESULTS

Including the nonlinear field errors in the triplets and the head-on beam-beam interactions at IP1 and IP5, we studied the evolution of beam sizes and the dynamics of beam centroids for various beam-beam parameters ξ. Note that in the current design of LHC, $\xi=0.0034$. For $\xi<0.03$, no significant emittance growth was found in over 10^5-turn trackings. Figure 2 plots the evolution of horizontal rms emittance in the first 2×10^4 turns for different ξ, and shows that the beam-beam instability occurs when $\xi>0.03$. Such a beam-beam instability can be characterized, as shown in the following, by an unstable oscillation of beam centroids and a significant growth of beam size. A plot of the vertical emittance or the emittance of the counter-rotating beam also show similar behaviors. Within the time scale of observation, there is clearly a threshold of the beam-beam parameter (ξ_c) for the beam-beam instability. For the current version of the LHC collision lattice with two interaction points, $\xi_c\simeq0.03$.

A. Unstable beam-centroid motion

With initially centered beams, no significant beam-centroid motion is observed for $\xi<\xi_c$. When $\xi>\xi_c$, however, the phase-space area near the origin becomes unstable for beam centroids, and the beam-beam interactions induce an unstable off-center oscillation of the beams. Figures 3 and 4 plot two typical cases of the unstable motion of one beam centroid for $\xi=0.032$ and 0.04, respectively. A similar plot for the counter-rotating beam shows that two beams oscillate oppositely (dipole oscillation) due to the conservation of the beam transverse momentum. It can be seen from Figs. 3 and 4 that the unstable motion of beam centroids consists of sudden jumps of the oscillation amplitude that are in distinct contrast to the slow increase of the amplitude observed most of the time. Such a combination of a sudden jump and a slow increase of the amplitude is the characteristic of chaotic transport in phase space [19–21]. In Fig. 5, the trajectory of beam centroids is plotted in the horizontal phase space for the cases of Figs. 3 and 4. In both cases the phase space contains nearly regular regions and fully developed chaotic regions. The nearly regular regions consist of bands of resonance and remnants of invariant manifolds that are partial barriers to globally unstable motions, and the fully developed chaotic regions are between the nearly regular bands. Due to a slow chaotic transport near the remnants of invariant manifolds, beam centroids have to spend a long time in a nearly regular band before they wend their way through those partial barriers. After crossing a nearly regular band, beam centroids can quickly pass through a fully developed chaotic region and reach the next nearly regular band. The amplitude of the motion of beam centroids therefore suddenly jumps. A comparison between horizontal and vertical motions of beam centroids in Figs. 3 and 4 shows that in a nearly regular band the dynamics of beam centroids is nearly two dimensional in the x-p_x plane, while in a chaotic region it becomes four dimensional in both x-p_x and $y-p_y$ planes. It should be noted that the asymmetry in the horizontal and vertical dynamics of beam centroids is due to the different horizontal and vertical betatron tunes. A simple exchange of the horizontal and vertical tunes can switch the horizontal and vertical dynamics, which suggests that the onset of the beam-beam instability could strongly depend on the working point

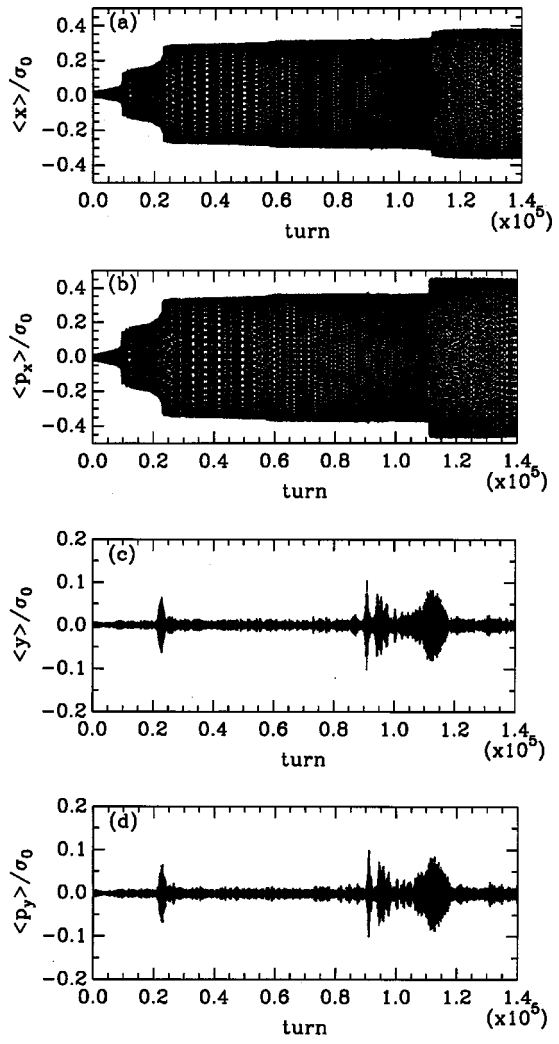

FIG. 3. The unstable motion of beam centroids in transverse phase space for $\xi=0.032$, where $\langle x\rangle$, $\langle p_x\rangle$, $\langle y\rangle$, and $\langle p_y\rangle$ are the normalized coordinates and momenta averaged over each bunch of particles. The initial beams are centered Gaussian beam with standard deviation σ_0. Multipole field errors in the triplets without IR correctors are included in the tracking.

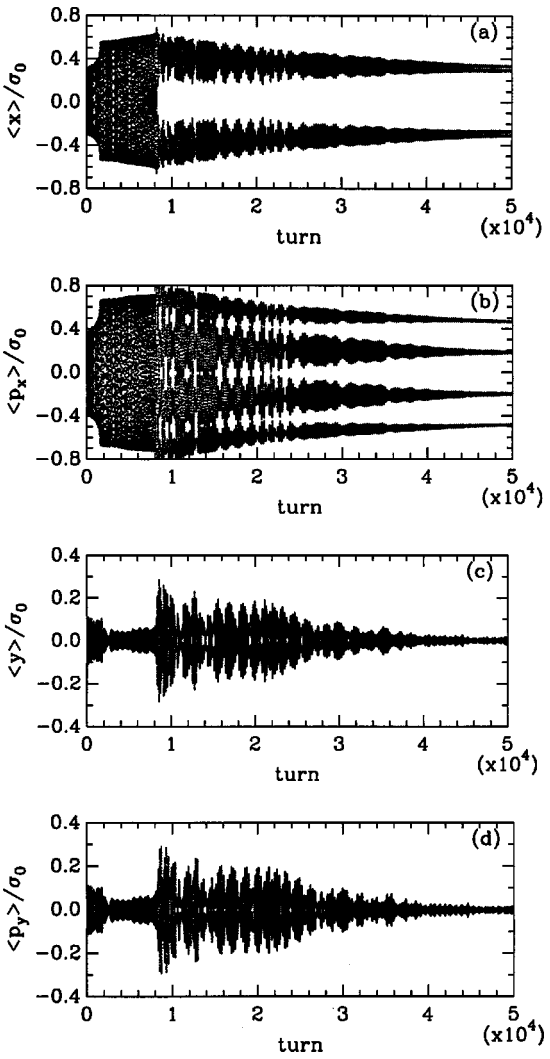

FIG. 4. The same as in Fig. 3, but for $\xi=0.04$.

of a collider. In the case of $\xi=0.04$, beam centroids eventually cross the separatrix of the fourth-order resonance, and are then trapped in the resonance [Figs. 4 and 5(b)]. For $\xi=0.032$, beam centroids are able to cross the fourth-order resonance [Figs. 3 and 5(a)]. It should be noted that the appearance of the strong fourth-order resonance is a consequence of the collective beam-beam effect, since with the strong-weak model in Eq. (3) this resonance should not appear in that phase space location with the given beam-beam parameter.

For a nonlinear system of interest, usually the stronger the nonlinear perturbation, the more severe the breakup of invariant manifolds. The strength of the nonlinearity can therefore affect the chaotic transport rate, which can be used to test the interpretation of the unstable beam-centroid oscillation based on chaotic transport. First, a comparison between Figs. 3 and 4 shows that the stronger the beam-beam interaction is, the earlier the amplitude jumps occur. This indicates that the transport rate of the beam-centroid motion increases, in general, with the strength of beam-beam interactions. Second, the inclusion or exclusion of the multipole field errors in the lattice should also expedite or delay the amplitude jumps. Figure 6 plots the motion of beam centroids without the multipole field errors in the triplets for $\xi=0.04$. A comparison between Figs. 4 and 6 shows that the nonlinear fields in the lattice indeed enhance the chaotic motion of beam centroids. On the other hand, when $\xi<\xi_c$, the phase-space area near the origin of the motion of beam centroids contains invariant manifolds that prevent the global instability. Figure 7 plots the motion of beam centroids for $\xi=0.0136$, with both beams being initially off-centered. It shows that even with off-centered beams, no unstable beam-centroid motion is developed for $\xi<\xi_c$.

It should be noted that for two mathematically symmetric (perfect round) beams centered at the origin in phase space [$\rho(-x,y)=\rho(x,y)$ and $\rho(x,-y)=\rho(x,y)$ in Eq. (1)], the net beam-beam force on the beam centers of mass is always zero, and no centroid motion can be developed in the case of linear lattice. When $\xi>\xi_c$, however, the origin becomes an unstable point for the beam centroids, and any fluctuation on the symmetry of the beams can develop into an unstable beam-centroid oscillation. Similar to real beams, the initial beams used in the simulation are only statistically symmetric, i.e., the beams are overall symmetric, but individual par-

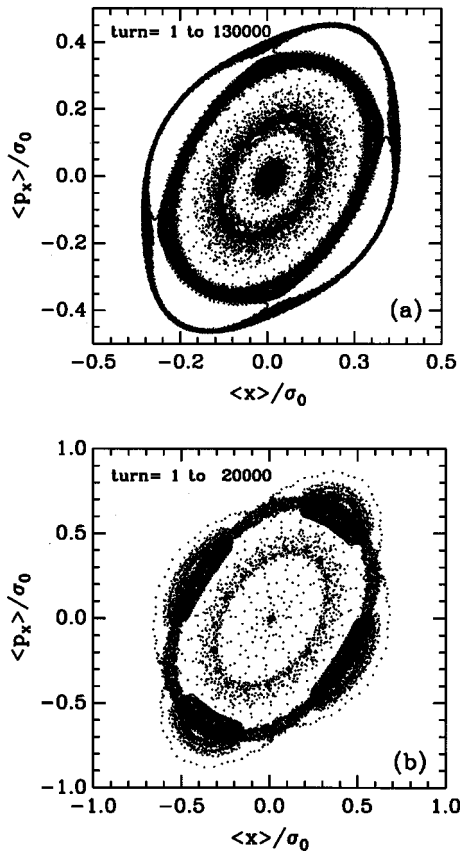

FIG. 5. The horizontal phase-space plot of the motion of beam centroids. Beam-beam interactions at IP1 and IP5 and multipole field errors in the triplets without IR correctors are included in the tracking. (a) $\xi=0.032$, and the trajectory of the first 130 000 turns is plotted. (b) $\xi=0.04$ and the trajectory of the first 20 000 turns is plotted.

ticles in the beams are not one-to-one symmetric in phase space. The lack of perfect symmetry in real beams or numerical beams is therefore the initial fluctuation that induces the beam-beam instability when $\xi>\xi_c$.

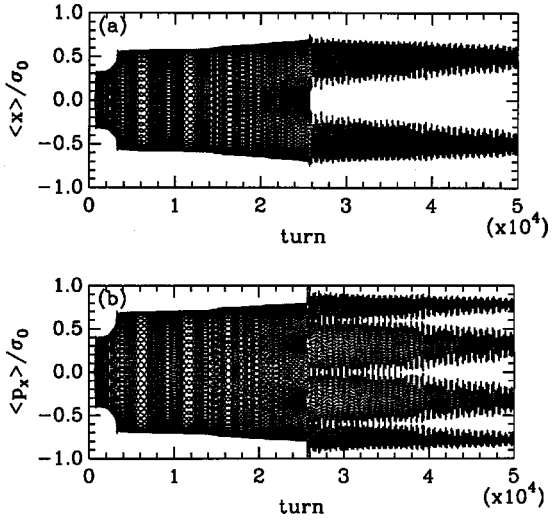

FIG. 6. The same as in Fig. 4, but without multipole field errors in the triplets.

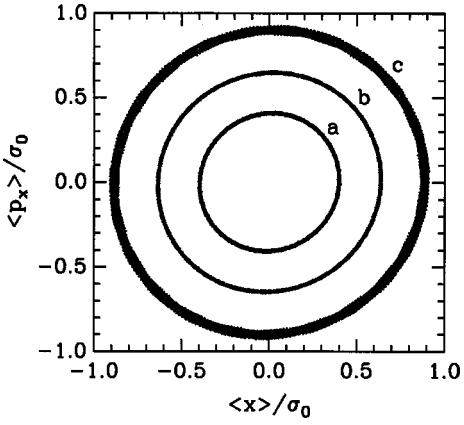

FIG. 7. Horizontal phase-space plot of the motion of beam centroids from a turn of 2000 to a turn of 20 000 for $\xi=0.0136$. Both beams are initially off-centered by (a) $0.5\sigma_0$, (b) $0.75\sigma_0$, and (c) $1.0\sigma_0$.

B. Beam-size growth

The rms transverse beam sizes are the second-order moments of the beams that are defined by $\sigma_z=\sqrt{\langle(z-\langle z\rangle)^2+(p_z-\langle p_z\rangle)^2\rangle/2}$, where $z=x$ or y for horizontal or vertical beam sizes. In this study, the initial beams are two identical round Gaussian beam in four-dimensional normalized transverse phase space. The initial beam size is thus σ_0 in both horizontal and vertical directions. Due to the nonlinearities in the system, the initial distributions of the beams are mismatched with the invariant manifold of the initial phase space. Beam sizes increase during the first few hundred turns as a result of beam filamentation (see Fig. 2). After this initial beam filamentation, no significant beam-size growth is observed when $\xi<\xi_c$ while the onset of beam-beam instability results in an enhanced slow beam-size growth when $\xi>\xi_c$. Figure 8 plots the size of one beam as a function of turn number for the case of Fig. 3 ($\xi=0.032$) and is a typical example of the beam-size growth after the onset of the beam-beam instability. A similar plot for the counter-rotating beam shows a similar characteristic. When $\xi>\xi_c$, the growth of the beam size is found to consist of a smooth increase with small jumps. A comparison between Figs. 3 and 8 shows that each jump in beam size corresponds to a sudden increase in the oscillation amplitude of beam centroids. Moreover, the growth rate of the smooth beam-size growth (the slop of $\sigma_{x,y}$) increases with the oscillation amplitude of beam centroids. When beam centroids are trapped

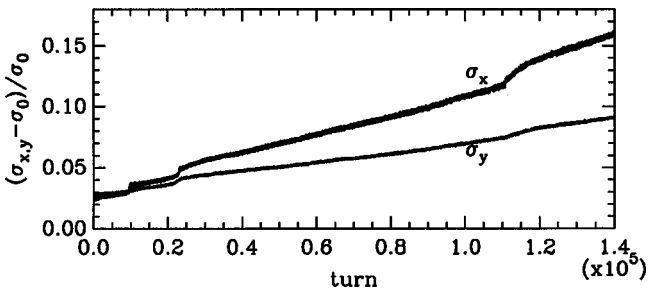

FIG. 8. Evolution of the rms beam size for the case of Fig. 3. The upper curve is the horizontal beam size, and the lower one the vertical beam size.

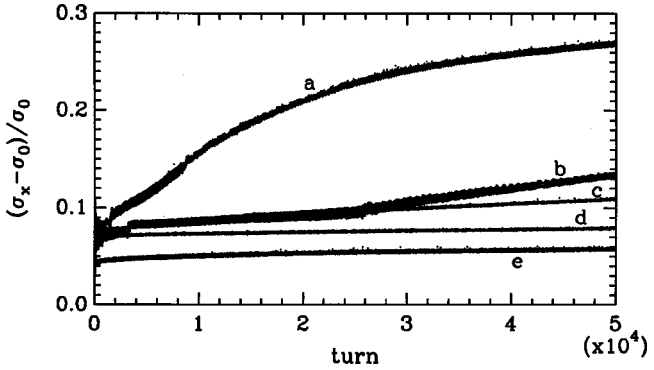

FIG. 9. Evolution of the horizontal rms beam size for $\xi=0.04$. The simulation was done with (a) multipole field errors in the triplets and without IR correctors (the case of Fig. 4); (b) the linear lattice (the case of Fig. 6); (c) the situation is the same as in (a), but with the beam-centroid motion removed in each turn with feedback; and (d) the situation is the same as in (b), but with the beam-centroid motion removed in each turn with feedback. (e) Strong-weak beam-beam simulation in the same situation as (a).

into a resonance, on the other hand, the growth of beam sizes gradually slows down—as shown by the curves in Figs. 9 and 10, in which $\sigma_{x,y}$ are plotted for the case of Fig. 4 ($\xi=0.04$).

To examine the effect of nonlinear field errors in the lattice on the beam-size growth, in Figs. 9 and 10 we also plot $\sigma_{x,y}$ for the case of Fig. 6, in which the beam-beam simulation was conducted on the linear LHC lattice with $\xi=0.04$. A comparison between curves *a* and *b* in Figs. 9 and 10 shows that the growth of beam sizes is significantly enhanced by the nonlinear field errors. Such an enhancement can be understood as particles with large amplitudes in the tails of the distributions become globally unstable due to field errors. To check the validity of the strong-weak simulation of the beam-beam effects, $\sigma_{x,y}$ were also calculated with a strong-weak simulation by using Eq. (3), and compared with the results of the strong-strong simulation. Curve *e* in Figs. 9 and 10 is the case of $\xi=0.04$ including the field errors in the triplets. A comparison between curves *a* and *e* in Figs. 9 and 10 shows that the strong-weak model of beam-beam interaction is not suitable for a study of the beam-size growth due to the beam-beam effects in proton-proton colliders.

During the operation of a hadron collider, the motion of beam centroids can be easily detected and eliminated with feedback. Similar beam-beam simulations were therefore

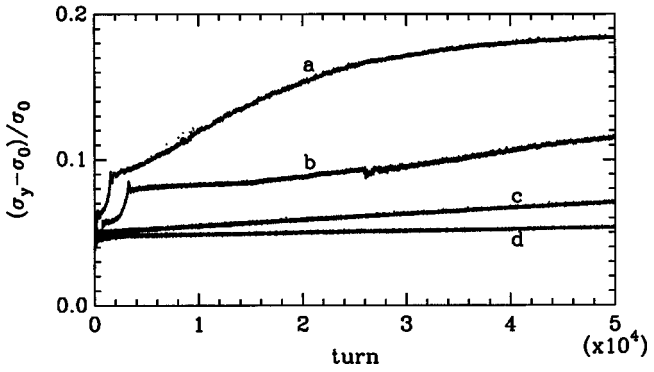

FIG. 10. The same as in Fig. 9, but for the vertical beam size.

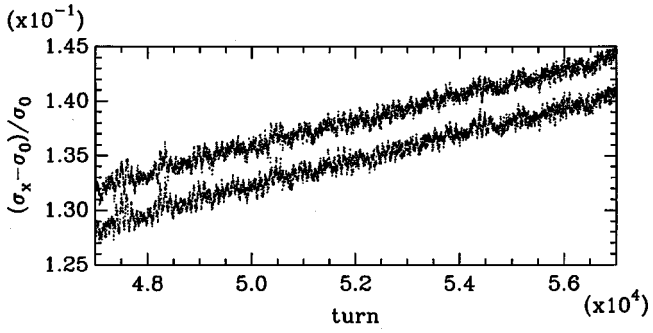

FIG. 11. A blowup of curve *b* in Fig. 9.

also conducted for $\xi>\xi_c$, with a feedback for the beam-centroid oscillation. It was found that the beam-size growth was largely suppressed by the elimination of unstable beam-centroid motion (curves *c* and *d* in Figs. 9 and 10). The beam-size growth after the onset of the beam-beam instability is therefore due mainly to the unstable oscillation of the beam centroids. As beam centroids circulate around the origin of phase space, the filamentation of the beams can result in a growth of beam sizes as the beams gradually spread along invariant manifolds in the phase space. However, in the case without feedback, the number of particles escaping to the tails of the distributions during the tracking is much larger than that in the case with feedback. Since the filamentation itself does not result in the escape of particles across invariant manifolds, the filamentation of the beams may not be the only cause of the enhanced beam-size growth after the onset of the beam-beam instability.

One phenomenon of coherent beam-beam effects in electron storage-ring colliders is the coherent oscillation of beam sizes, in which the sizes of two counter-rotating beams vary periodically from turn to turn. Usually, such an oscillation is anticorrelated, i.e., one beam is dense while the other is hollow [6,8]. It is clear from Fig. 11 that there is a period-2 oscillation of beam sizes after the onset of the unstable beam-centroid oscillation of hadron beams, even though the variation of beam sizes during this oscillation is only about 0.4% of beam sizes. A plot of both beam sizes as a function of the turn number shows that two counter-rotating beams oscillate correlatively (in phase). After eliminating the beam-centroid oscillation with feedback, however, the oscillation of the beam sizes disappears. Such a beam-size oscillation in hadron colliders is therefore a result of the beam-centroid oscillation, and is not the same spontaneous oscillation as that in electron storage-ring colliders. Since the centroids of two counter-rotating beams oscillate correlatively due to the conservation of the beam transverse momentum, the oscillations of beam sizes are also correlated in hadron colliders.

IV. SUMMARY

Collective beam-beam effects in hadron colliders were studied with a strong-strong beam-beam simulation on LHC with working points of $\nu_x=0.31$ and $\nu_y=0.32$. Multipole field errors in the lattice and beam-beam interactions at two high-luminosity interaction points were included in the simulation. A threshold of the beam-beam parameter ξ_c was found for the onset of the beam-beam instability of hadron beams. When $\xi<\xi_c$ no significant emittance growth due to beam-beam interactions was observed; however when $\xi>\xi_c$, a beam-beam instability characterized by an unstable oscillation of beam centroids and an enhanced beam-size

growth occurs. Due to the onset of the beam-beam instability, the phase-space area nearby the origin becomes unstable for beam centroids, and two initially centered counter-rotating beams develop a spontaneous unstable off-center oscillation. The dynamics of the unstable beam-centroid oscillation has characteristics typical of chaotic transport in phase space, and the slow beam-size growth is significantly enhanced by this unstable beam-centroid oscillation. The growth rate of beam sizes is found to increase with the oscillation amplitude of beam centroids. The nonlinear field errors in the lattice, on the other hand, could significantly enhance the instability of the beam-centroid motion and the growth of beam sizes. This study showed that the beam-beam instability of hadron beams could be effectively suppressed by an elimination of the beam-centroid motion with feedback. After the removal of the unstable beam-centroid oscillation, the enhanced beam-size growth is largely eliminated, and the nonlinear field errors in the lattice become dominant nonlinearities to cause the slow beam-size growth. For the current design of LHC, ξ_c is about nine times the size of the nominal beam-beam parameter when two interaction points (IP1 and IP5) are considered. If two additional interaction points (IP2 and IP8) are also used for the experiment, the beam-beam parameter of LHC could be much closer to its threshold. By using feedback to control the beam-beam instability, however, the head-on beam-beam effects should not be a limit for future luminosity upgrades in LHC. It is, however, clear that in weak-strong beam-beam simulations long-range beam-beam interactions are important to the beam-size growth [22,23]. A thorough study of the LHC beam-beam limit should also include long-range beam-beam effects in the strong-strong beam-beam simulation.

One important characteristic of the collective beam-beam effects in hadron colliders is the nonexistence of steady states for coherent oscillations, as shown in this study. Due to a large damping time scale, the dynamics of particle distributions of hadron beams are practically governed by the Hamiltonian dynamics that is characterized by a chaotic transport of beam particles from the beam core to the tails due to nonlinear perturbations. Because of this slow particle escape and the lack of fluctuations dissipation, the particle distributions may not be able to reach any equilibrium or steady states during the luminosity lifetime, and this makes the dynamics of a transient state (time evolution) of beam distributions important to hadron beams. It is therefore important to recognize the difference between hadron and electron beams when attempting to develop theoretical models for the collective beam-beam effects of hadron beams.

The many interesting features observed in this work suggest that collective beam-beam instabilities in high-intensity hadron beams may in fact be much more complicated than we have been accustomed to thinking. Many questions arising from this study need to be addressed, including the dependence of ξ_c on the system parameters, especially the betatron tunes and the mechanism of a beam-size growth after the onset of the beam-beam instability. It is thus worthwhile to conduct a more thorough study of numerical simulations as well as a theoretical modeling of the beam-beam instability of hadron beams. Since a very large number of macroparticles is required for the strong-strong beam-beam simulation of hadron beams, such a study with numerical simulations is hardly feasible unless parallel computing is employed with high-power multiprocessor computers.

ACKNOWLEDGMENTS

The authors would like to thank Professor S. Ohnuma for many stimulating discussions. This work was supported by the National Science Foundation under Grant No. PHY-9722513, and the University of Kansas General Research Fund. We would like to thank the Center for Advanced Scientific Computing at the University of Kansas for the use of the supercomputer.

[1] *Nonlinear Dynamics and the Beam-Beam Interaction*, edited by M. Month and J. C. Herrera, AIP Conf. Proc. No. 57 (AIP, New York, 1979).
[2] CERN Courier, May 1994, p. 20.
[3] A. W. Chao, M. A. Furman, and K. Y. Ng, in *Proceedings of the European Particle Accelerator Conference, Rome, 1988*, edited by S. Tazzari (World Scientific, Singapore, 1989), p. 175.
[4] N. S. Dikansky and D. V. Pestrikov, Part. Accel. **12**, 27 (1982).
[5] A. W. Chao and R. D. Ruth, Part. Accel. **16**, 201 (1985).
[6] S. Krishnagopal and R. Siemann, Phys. Rev. Lett. **67**, 2461 (1991).
[7] B. Podobedov and R. Siemann, Phys. Rev. E **52**, 3066 (1995).
[8] S. Krishnagopal, Phys. Rev. Lett. **76**, 235 (1996).
[9] E. B. Anderson, T. I. Banks, and J. T. Rogers, in *Proceedings of the 1999 Particle Accelerator Conference* (IEEE, New York, 1999).
[10] J. Shi and S. Ohnuma, Phys. Rev. E **47**, 4405 (1993).
[11] D. Yao and J. Shi, ST Accel. Beams **1**, 084 001 (1998).
[12] Y. I. Alexahin, CERN Report No. CERN/SL/96-064 (1996).
[13] K. Yokoya, Y. Funakoshi, E. Kikutani, H. Koiso, and J. Urakawa, Part. Accel. **27**, 181 (1990).
[14] C. K. Birdsall and A. B. Langdon, *Plasma Physics via Computer Simulation* (McGraw-Hill, New York, 1985).
[15] R. W. Hockney and J. W. Eastwood, *Computer Simulation Using Particles* (McGraw-Hill, New York, 1981).
[16] The LHC Study Group, *The Large Hadron Collider Conceptual Design*, CERN Report No. CERN/AC/95-05 (LHC).
[17] Different versions of reference harmonic for LHC IR quadrupoles are available on the US-LHC project web page: http://www/agsrhichome.bnl.gov/LHC
[18] W. Fischer and J. Wei, *Proceedings of the Workshop on LHC Interaction Region Correction Systems*, Brookhaven National Lab Report No. BNL-52575 (1999).
[19] J. D. Meiss, Rev. Mod. Phys. **64**, 795 (1992), and references therein.
[20] S. Wiggins, *Chaotic Transport in Dynamical Systems* (Springer-Verlag, Berlin, 1992).
[21] J. Shi, Phys. Rev. Lett. **76**, 3971 (1996).
[22] Y. Papaphilippou and F. Zimmermann, in *Proceedings of the LHC99 Workshop on Beam-Beam Effects in Large Hadron Colliders*, Cern Report No. CERN/SL/99-039 (1999).
[23] F. Schmidt, H. Grote, and L. Leunissen (unpublished).